Effect of Sensitizer Structure and TiO2 Protonation on Charge Generation in Dye-Sensitized Solar Cells

ARTICLE *in* THE JOURNAL OF PHYSICAL CHEMISTRY C · JANUARY 2014

Impact Factor: 4.77

4 AUTHORS, INCLUDING:

Enrico Ronca

Princeton University

16 PUBLICATIONS **384** CITATIONS

SEE PROFILE

Mariachiara Pastore

Italian National Research Council

50 PUBLICATIONS **1,243** CITATIONS

SEE PROFILE

Filippo De Angelis

Università degli Studi di Perugia

263 PUBLICATIONS **11,162** CITATIONS

SEE PROFILE

THE JOURNAL OF PHYSICAL CHEMISTRY C

Article

pubs.acs.org/JPCC

Effect of Sensitizer Structure and TiO_2 Protonation on Charge Generation in Dye-Sensitized Solar Cells

Enrico Ronca,[†,‡] Gabriele Marotta,[†,‡] Mariachiara Pastore,*[,†] and Filippo De Angelis*[,†]

[†]Computational Laboratory for Hybrid Organic Photovoltaics (CLHYO), Istituto CNR di Scienze e Tecnologie Molecolari, via Elce di Sotto 8, I-06123 Perugia, Italy

[‡]Dipartimento di Chimica, Biologia e Biotecnologie, Università degli Studi di Perugia, via Elce di Sotto 8, I-06123 Perugia, Italy

ABSTRACT: We report a joint theoretical and experimental investigation on the effect of TiO_2 protonation on the interfacial electronic coupling and injection rates in organic dye-sensitized solar cells (DSCs). We model the electronic structure of different organic dye-sensitized TiO_2 cluster models at different degrees of surface protonation and experimentally show the enhancement in the photocurrent generation upon the acidic treatment of the substrate. By merging theory and experiments, we elucidate the role of TiO_2 protonation on the relative alignment and electronic coupling (injection rates) between the dye's lowest unoccupied molecular orbital and the semiconductor conduction band states, also in relation to the different electronic structure of the anchored dye (length of conjugation, conjugated vs not conjugated anchoring group). The photocurrent enhancement observed with TiO_2 protonation is attributed to a combined effect of both red-shifted absorption of the protonated TiO_2 films and to an overall improvement in the interfacial charge generation

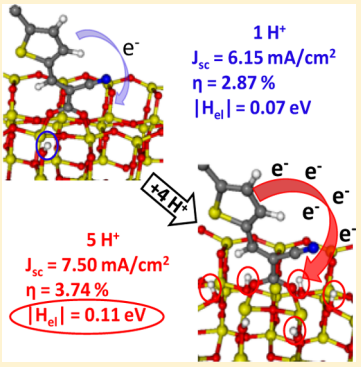

1. INTRODUCTION

Dye-sensitized solar cells (DSCs)[1−4] have attracted increasing attention as a promising alternative to conventional silicon-based solar cells because of their relatively high conversion efficiencies and low production costs. Ruthenium polypyridyl complexes have been the most extensively studied dye sensitizers, with conversion efficiency exceeding 11%.[2,4,5] Recently, Zn(II)-porphyrins have reached even higher efficiency when coupled to Co(II)/Co(III) redox shuttles, exceeding 12%.[6] Despite their high efficiency and long-term stability, metal complexes are not the ideal candidates for cost-effective and environmental-friendly photovoltaic devices. For these reasons in recent years the study of fully organic dyes has attracted considerable interest.[4,7−11] The molecular structure of organic dyes usually follows the donor-π bridge-acceptor (D-π-A) pattern, with the acceptor group anchored to the semiconductor surface, ensuring an ultrafast electron injection into the semiconductor conduction band (CB) upon the intramolecular charge separation. DSCs employing these dyes have obtained efficiencies close to 10%[12−15] with standard I^-/I_3^- electrolyte, whereas in conjunction with novel ferrocene or cobalt-based electrolytes, they even achieved performance superior to that of Ru(II) dyes.[6,16−18]

The solar energy-to-electricity conversion efficiency η of a DSC is determined by the short circuit photocurrent density (J_{sc}), the open circuit voltage (V_{oc}), the fill factor (FF) of the cell, and the intensity of the incident light (I_s), namely

$$\eta = J_{sc} V_{oc} \mathrm{FF} / I_s \tag{1}$$

The open circuit voltage represents the difference between the quasi-Fermi level of the semiconductor under illumination and the redox potential of the electrolyte. Recently, several works have been published to understand the *indirect* effect of the organic dye structure on the V_{oc}, which, we recall, is directly affected by the charge recombination processes.[19−24] The photocurrent density is instead a quantity related to the electron dynamics phenomena occurring in the working device, depending both on the dye light-harvesting and on the kinetics of the electron injection, dye regeneration, and charge transport within the cell. We can thus consider the J_{sc} as a quantity *directly* dependent on the dye properties.

The first and most important electron-transfer process occurring in a DSC is the charge injection from the photoexcited dye to the CB of the semiconductor. The growing interest in the study of this phenomenon is due to the recent development of very accurate techniques[25] capable of delivering information in the femtosecond time scale.[26−31] From the theoretical side, the description of excited-state electron injection into wide-bandgap semiconductors was first modeled by Marcus and Gerischer.[32−34] Under the weak coupling assumption, the rate constant (k_{inj}) for the electron transfer from a single sensitizer's d state to the many acceptor states k of the semiconductor can be expressed using the Fermi Golden Rule through the relation

$$k_{inj} = \frac{2\pi}{\hbar} \sum_k |V_{dk}|^2 \rho(\varepsilon_k) \tag{2}$$

Special Issue: Michael Grätzel Festschrift

Received: January 15, 2014
Revised: February 28, 2014

   dx.doi.org/10.1021/jp5004853 | J. Phys. Chem. C XXXX, XXX, XXX−XXX

where $\rho(\varepsilon_k)$ is the density of semiconductor acceptor states (DOS) at the energy ε_k, V_{dk} the electronic coupling matrix element between the diabatic donor d state and the kth acceptor state in TiO_2, and $\hbar$ Planck's constant. The quantum yield for electron injection η_{inj} (fraction of photons adsorbed by the dye that result in electron injection into the CB of the semiconductor) is determined by

$$\eta_{\mathrm{inj}} = \frac{k_{\mathrm{inj}}}{k_{\mathrm{inj}} + k_0 + k_{\mathrm{q}}} \tag{3}$$

where k_0 is the rate constant for radiative and nonradiative decay of the excited state of isolated dye molecules and k_q represents all possible quenching pathways of the dye excited state in the device apart from electron injection.

The great success obtained by ruthenium dyes in the DSC field is at least in part due to their high electron injection quantum yields,[35−40] arising from the high values of the electron injection rates (~100 ps) but also from the long lifetimes (from tens to hundreds of nanoseconds) of the lowest triplet state (the most involved in the charge injection process thanks to the ultrafast intersystem crossing) that strongly reduce the term k_0 in eq 3.[40] In metal complexes, electron injection is also favored by the low values of the recombination rate constant due to an efficient electron−hole separation and by their peculiar adsorption geometry, which effectively reduces the interfacial aggregation phenomena.[40] On the other hand, for organic dyes the thermalization to the triplet state is much slower than the injection and emission processes, and then the system is forced to transfer the electron directly from the singlet state. Despite the fact that the injection rate from the singlet is faster than that from the triplet state (<60 ps), the singlet lifetime can be about 20-fold smaller, resulting in a significantly increased competition between the injection process and the radiative decay, with a consequent lowering in the quantum yields.[40] In addition, organic dyes show faster recombination of the injected electron with the oxidized sensitizer with respect to metal complexes, possibly caused by a generally closer localization of the dye highest occupied molecular orbital (HOMO) to the semiconductor surface,[40] also favored by particular adsorption configurations.[22,41] It is thus clear that a deep comprehension of the parameters favoring the electron injection rate is of fundamental importance for enhancing the efficiencies in DSCs, particularly when organic dyes are employed.

The energy difference between the excited-state oxidation potential (ESOP) of the dye and the TiO_2 CB energy governs the thermodynamics of electron injection: provided that the dye's excited-state energy remains roughly constant, an upshift (negative)/down-shift (positive) of the semiconductor CB energy will result in a reduction/increase of the driving force due to variation of $\rho(\varepsilon)$ in eq 2 and thus of the efficiency of the electron injection. It is well-known that several factors,[42,43] such as the local pH,[44] the concentration of potential-determining ions (e.g., Li^+),[45−51] and possibly in relation to acid−base equilibria, also on the nature of the electrolyte solvent,[46,52] may influence the position of the CB edge. In particular, proton adsorption to metal oxide surfaces shifts the position of the valence band edge maximum and conduction band edge minimum away from the vacuum level by 59 mV per pH unit, following the Nernst equation. Similar pH effects have been reported also for sensitized nanocrystalline TiO_2 films,[53−57] where surface protonation has been effectively employed to positively shift the conduction band edge thus improving J_{sc}.[42,57−61] The effect of surface protonation, as well as that of other potential determining ions, on the measured J_{sc} is actually more complicated than a mere shift in the semiconductor CB because also the dye's excited states, in particular its nature, its energy, and the coupling with the TiO_2 CB states, can also be influenced significantly.[62−65]

Here, integrating and extending our previous works on the effect of the cationic additives at the organic dye/TiO_2 interface[62] on one side and on the dye absorption spectral changes upon substrate protonation on the other side,[66] we model the electronic structure of different organic dye-sensitized TiO_2 surface models under varying protonation conditions and experimentally demonstrate the enhancement in photocurrent generation upon TiO_2 protonation in DSC devices. By merging theory and experiments, we shall elucidate the role of the TiO_2 protonation on the relative alignment and electronic coupling (injection rates) between the dye's excited state and the semiconductor CB states, also in relation to the different electronic structure of the anchored dye (Figure 1). Finally, on the basis of our calculations, we attribute the observed photocurrent enhancement to a combined effect of red-shifted absorption of the dye-sensitized TiO_2 film[67] coupled to an overall improvement in the interfacial charge generation.

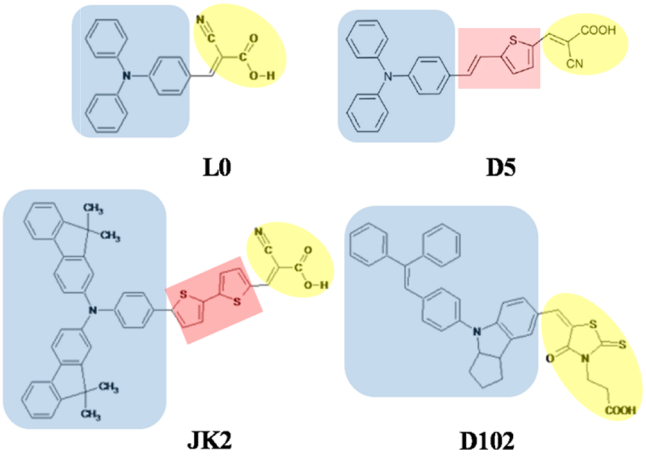

Figure 1. Molecular structures of the L0, D5, JK2, and D102 dyes.

The paper is organized as follows: In the next section a brief summary of the theoretical strategies used for the evaluation of the injection rates (the Newns−Anderson method[68] and a new diabatic-like approach developed by Thoss et al.[69,70]) and of the electronic couplings is reported. Then, a fine analysis on the effects of the progressive TiO_2 protonation on the charge injection kinetic as a function of the modifications of the dye electronic structure will be presented. In the last part of the work we compare the discussed theoretical results with experimental data obtained by UV−vis spectra and incident photon-to-current efficiency (IPCE) measurements.

2. COMPUTATIONAL DETAILS AND THEORETICAL MODELS

Our calculations are based on two prototypical, cyanoacrylic-based conjugated sensitizers (Figure 1) differing for the length of the π spacer, namely, L0,[4,7,41] in which the triphenylamine donor is directly bound to the cyanoacrylic acceptor, and JK2, which is instead constituted by a substituted triphenylaminic donor linked to the cyanoacrylic moiety by two thiophene rings.[11,71−73] For the latter we also analyzed a different configuration, obtained by

dx.doi.org/10.1021/jp5004853 | J. Phys. Chem. C XXXX, XXX, XXX−XXX

twisting of 90° the C−C bond connecting the cyanoacrylic anchoring and thiophene groups (JK2-T, see below), to quantify the effects due to the breaking of the electron conjugation. Then, we also consider a nonconjugated dye, D102, composed of a substituted indoline donor group directly bound to a rhodanine-3-acetic anchoring unit.[11,82,83]

The considered sensitizers have been anchored on the TiO_2 surface by the carboxylic group in the bridged bidentate adsorption mode (Figure 2).[10,74] In this configuration the carboxylic group interacts with two surface titanium atoms upon transferring its proton to one of the TiO_2 oxygens.

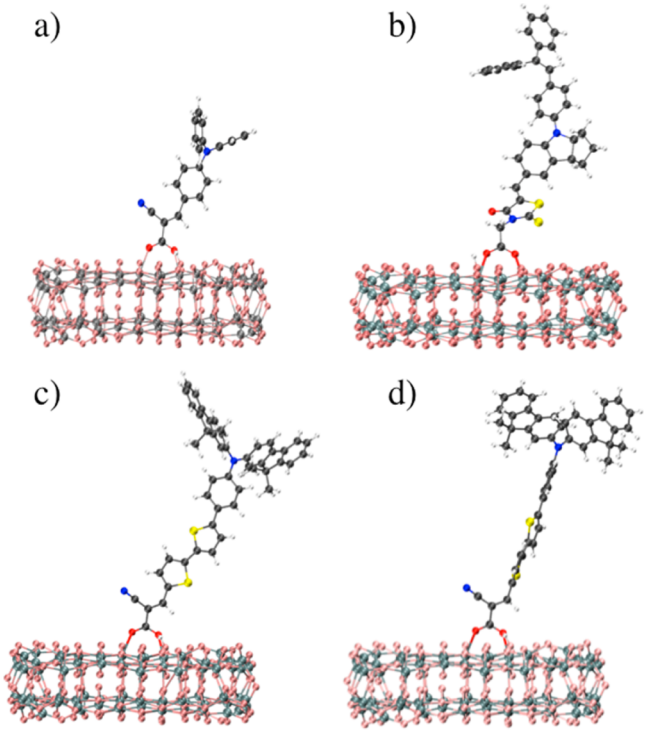

Figure 2. Optimized geometries of the L0 (a), D102 (b), JK2 (c), and JK2-T (d) dyes adsorbed onto the $(TiO_2)_{82}$ cluster in bridged bidentate (BB) anchoring geometry.

The TiO_2 surface has been simulated through the use of a $(TiO_2)_{82}$ cluster,[75] obtained by "cutting" in the appropriate way an anatase slab exposing the majority (101) surface.[76] This cluster model can be regarded as a good compromise between accuracy and computational cost, nicely reproducing the main electronic properties of TiO_2 nanoparticles.[77−80] To model the surface protonation we added on the TiO_2 cluster surface an increasing number of protons, as shown in Figure 3. The first proton has been placed at the center of the cluster, close to the dye's anchoring positions, while the remaining four H^+'s have been progressively added at the cluster corners, following the order specified by the numbers in Figure 3.

The dye@$(TiO_2)_{82}$ ground-state equilibrium geometries were obtained in the gas phase using density functional theory (DFT) with the ADF program package[81] employing the PBE exchange correlation functional[82] with the TZP (DZP) basis set for Ti (H,C,N,O,S) atoms.

To have a fast estimation of the electron injection times between the sensitizer and the semiconductor surface, we employ the Newns−Anderson model[68,83] in the formulation used by Persson et al.[84−87] This approach allows the evaluation of

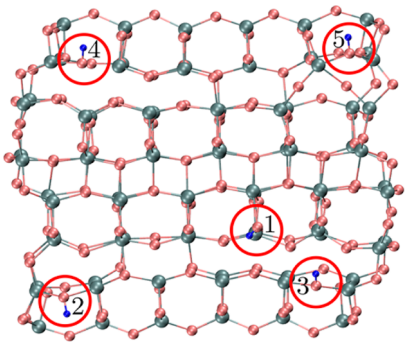

Figure 3. Schematic of the adsorption position of protons on the $(TiO_2)_{82}$ cluster.

the effects of the adsorption on the sensitizer electronic levels (generally only the dye LUMO is analyzed), characterizing them in terms of an energy shift relative to the free dye and a lifetime broadening, $\hbar\Gamma$. This lifetime broadening is well-described by a Lorentzian distribution resulting from the decay of the dye excited state, here approximated by the dye LUMO, coupled to the continuum of the TiO_2 CB states.[83] To calculate these quantities we need to evaluate the projected density of states (PDOS) relative to the dye's LUMO in the complex. When the system's molecular orbitals in a certain atomic basis are expanded, the contributions p_i to the dye's LUMO PDOS are defined by the relation

$$p_i = \frac{\sum_j^{A\in \mathrm{dye}} (c_{ij}^A)^2}{\sum_j^n (c_{ij}^A)^2} \tag{4}$$

where c_{ij}^A are the expansion coefficients of the complex molecular orbitals on the basis function of atom A belonging to the dye.

The center of this distribution corresponds to the energy of the sensitizer's LUMO adsorbed on TiO_2, $E_{LUMO}(ads)$, and it can be calculated through the relation

$$E_{LUMO}(ads) = \sum_i p_i \varepsilon_i \tag{5}$$

On the other hand, the width of the LUMO broadening can be estimated as a mean deviation of a distribution centered at the $E_{LUMO}(ads)$ energy value through the equation

$$\hbar\Gamma = \sum_i p_i |\varepsilon_i - E_{LUMO}(ads)| \tag{6}$$

The LUMO broadening gives a direct estimation of the electron transfer time that can be evaluated by $\tau(fs) = 658/\Gamma(meV)$.

The PDOS relative to the sensitizer's LUMO has been evaluated on the basis of single-point calculations performed at the DFT/B3LYP level of theory using the SVP basis set[88,89] on the ADF-optimized geometries. Solvation effects (acetonitrile) have been taken into account by means of the C-PCM[90,91] method as implemented in the Gaussian 09 (G09) suite.[92] The dye's PDOS has been plotted centering at each eigenvalue a Gaussian function with a standard deviation σ = 0.30 eV. At the same level of calculation we evaluated also the DOS for the TiO_2 cluster both in the absence and in the presence (PDOS) of the dye. Also in this case we used a broadening for the Gaussian functions equal to σ = 0.30 eV. To get an estimation of the energetic position of the TiO_2 CB edge, we performed a linear fitting of the low-energy profile in a range from 20% to 80% of the maximum height;[19] the intercept of this line with the energy axis

dx.doi.org/10.1021/jp5004853 | J. Phys. Chem. C XXXX, XXX, XXX−XXX

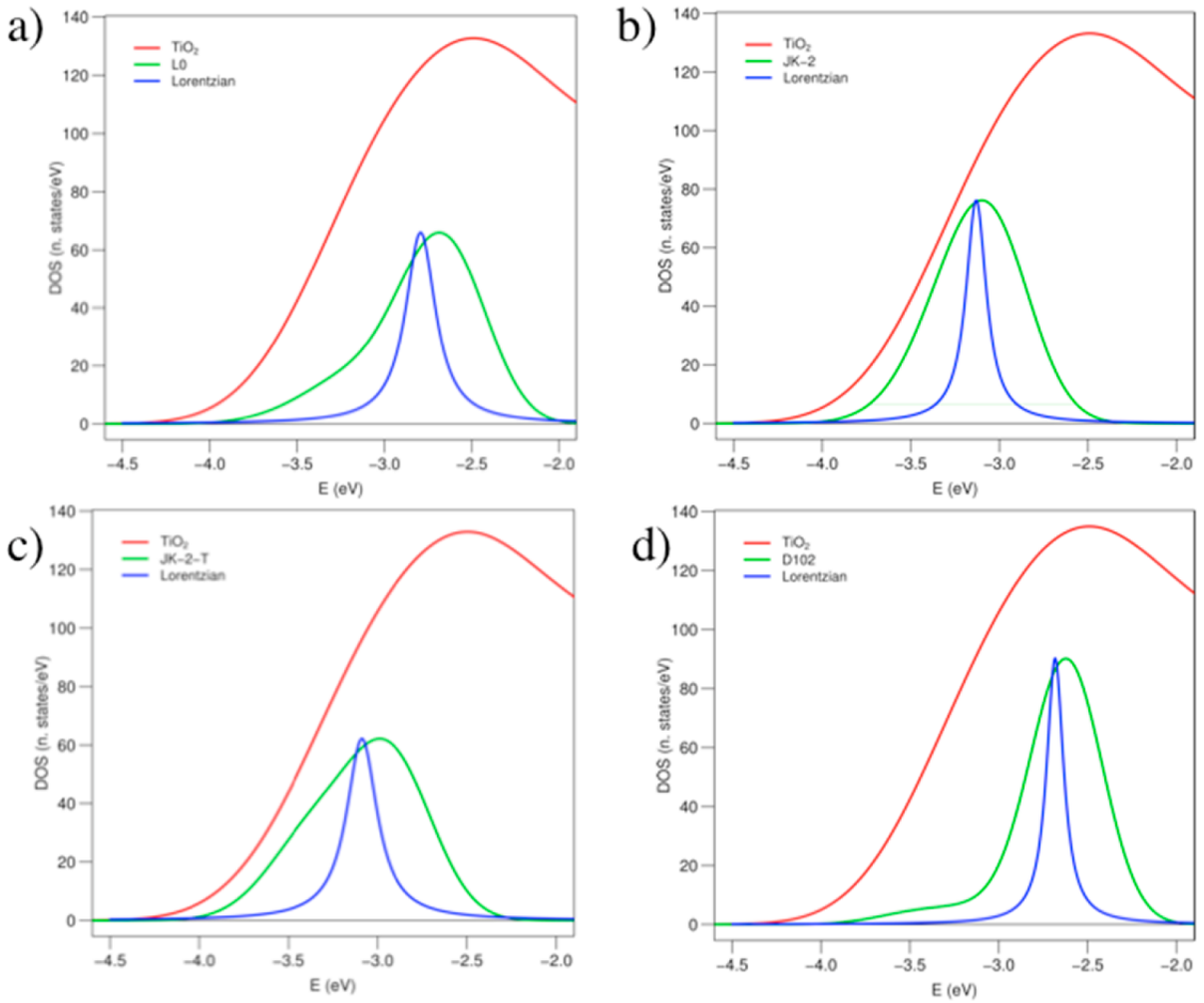

Figure 4. PDOS relative to the sensitizer and to TiO_2 and corresponding Lorentzian distribution of the dye's LUMO for L0 (a), JK2 (b), JK2-T (c) and D102 (d) in their neutral form (1H). The TiO_2 PDOS have been normalized; those corresponding to the sensitizer have been normalized and multiplied by 50; and the Lorentzian distributions have been normalized on the dye's PDOS maximum.

was taken as the CB edge. As discussed in ref 19, we have verified that the relative trends are weakly dependent on the choice of the fitting range.

The Newns−Anderson model described above, although relatively simple, does not allow the direct evaluation of the coupling between the dye and semiconductor states, leading directly to the injection time. To gain this information, we adopted the model recently developed and applied by Thoss et al.[69,70] This approach, based on the localization of the molecular orbitals of the entire complex on the donor (d) and acceptor (a) species, allows the expression of the Fock matrix of the interacting system (dye+TiO_2) in the following form:

$$\overline{F} = \begin{pmatrix} \overline{F}_{dd} & \overline{F}_{da} \\ \overline{F}_{ad} & \overline{F}_{aa} \end{pmatrix} = \begin{pmatrix} \varepsilon_{d1} & 0 & \cdots & & & \\ 0 & \varepsilon_{d2} & \cdots & & \overline{F}_{da} & \\ \vdots & \vdots & \ddots & & & \\ & & & \varepsilon_{a1} & 0 & \cdots \\ & \overline{F}_{ad} & & 0 & \varepsilon_{a2} & \cdots \\ & & & \vdots & \vdots & \ddots \end{pmatrix} \quad (7)$$

In this representation, the diagonal elements represent the energies of the localized sensitizer's states and those of the semiconductor cluster, while the off-diagonal blocks contain the coupling elements between dye and TiO_2 ($V_{dk} = (\overline{F}_{da})_{nk}$). The orbitals (indicated by $|\overline{\phi}^d_n\rangle$ and $|\overline{\phi}^a_n\rangle$, respectively) obtained by the separate diagonalization of the dd and aa blocks of the original F matrix are clearly different in principle from the dye's and semiconductor states. Despite this, for this kind of system, these localized orbitals are very similar to those of the corresponding isolated species comparing both the energies and shapes of the eigenvectors.[69,70]

3. EXPERIMENTAL DETAILS

For the device fabrication, following our previous work, we employed the prototypical push−pull D5 dye,[66] whose molecular structure is displayed in Figure 1 and which can be considered representative of the donor-π-acceptor type organic sensitizers.

3.1. Cell Fabrication and Characterization. Fluorine-doped tin oxide (FTO) glass (TEC-15, 2.2 mm thickness, Solaronix) was used for transparent conducting electrodes. The substrate was first cleaned in an ultrasonic bath using a detergent solution, acetone, and ethanol (each step was 15 min). The FTO glass plates were immersed into a 40 mM aqueous $TiCl_4$ solution at 70 °C for 30 min and washed with water and ethanol. After that a monolayer of opaque TiO_2 paste (Dyesol, 18NR-AO) was

dx.doi.org/10.1021/jp5004853 | J. Phys. Chem. C XXXX, XXX, XXX−XXX

Table 1. Calculated CB Energetic Position of the Bare TiO_2 at the Geometry It Assumes in the Complex (E_{CB}), Energy of the LUMO of the Dye Adsorbed on the Semiconductor (E_{LUMO}), CB Energy Position of the TiO_2 in the Presence of the Sensitizer ($E_{CB\text{-}complex}$), Bare TiO_2 DOS Value Extracted at E_{LUMO} (DOS), TiO_2 DOS Value Extracted at E_{LUMO} in the Presence of the Dye ($DOS_{complex}$), and Lorentzian Broadening ($\hbar\Gamma$) for the Investigated Systems in 1H Form

proton no.	E_{CB} (eV)	$E_{HOMO\_complex}$ (eV)	E_{LUMO} (eV)	$E_{CB\text{-}complex}$ (eV)	DOS (eV^{-1})	$DOS_{complex}$(eV^{-1})	$\hbar\Gamma$ (eV)
L0	−3.999	−5.622	−2.793	−3.845	122.3	122.2	0.210
JK2	−3.999	−5.105	−3.131	−3.844	96.9	89.6	0.141
JK2-T	−4.000	−5.013	−3.087	−3.859	101.5	96.2	0.209
D102	−4.000	−5.191	−2.683	−3.839	125.9	126.6	0.116

spread on the FTO glass plates by doctor blade. The TiO_2 layer film was treated in an ethanol chamber and dried for 5 min at 120 °C. The TiO_2 coated electrodes (active area, 0.2 cm^2) were gradually heated under air-flow at 325 °C for 5 min, 375 °C for 5 min, 450 °C for 15 min, and 500 °C for 15 min. After the sintering process, the TiO_2 film was again treated with 40 mM $TiCl_4$ solution then rinsed with water and ethanol. The electrodes were heated at 500 °C for 30 min and after cooling (80 °C) were immersed for 5 h in a sensitizing bath. This consisted of EtOH:THF (9:1) solutions of D5 dye in 0.2 mM concentration, with 10.0 mM of 3a,7a-dihydroxy-5b-cholic acid (CDCA) added. The effects of different acidic treatments can be investigated by immersing the photoanode into acid solutions of different concentration, as reported in ref 93. Here we compared devices produced in the absence of acidic treatment with those obtained by immersing the photoanode in a hydrochloric acid 0.1 M ethanol solution for two hours (at 80 °C) before the sensitization.[59] Counter electrodes were prepared by coating a FTO plate (TEC 15/2.2 mm thickness, Solaronix) with a drop of H_2PtCl_6 solution (2 mg of Pt in 1 mL of ethanol) and heating the FTO plate and solution at 400 °C for 15 min. The TiO_2 sensitized photoanode and Pt counter electrode were assembled into a sealed sandwich-type cell by a hot-melt ionomer film (Surlyn, 25 μm thickness, Dyesol). The electrolyte solution, the commercially available Iolitech ES-0004 HP, containing 1-butyl-3-methylimidiazolium iodide, iodine, guanidiniumthiocyanate, and *tert*-butylpyridine, in a mixture of valeronitrile and acetonitrile, was inserted by vacuum backfilling. Then, the hole was sealed by using additional Surlyn patch and a cover glass; finally, a conductive Ag-based paint was deposed at the electrical contacts.

Photovoltaic measurements were recorded by means of AM 1.5 solar simulator equipped with a Xenon lamp (LOT-ORIEL LS 0106). The power of incoming radiation, set at 100 mW/cm^2, was checked by a piranometer. $J-V$ curves were obtained by applying an external bias to the cell and measuring the generated photocurrent with a Keithley model 2400 digital source-meter, under the control of dedicated LabTracer 2.0 software. A black shading mask was employed to avoid the overestimation of the measured parameters.

3.2. Spectroscopic Study of Dye-Sensitized TiO_2 Layer. For the spectroscopic measurements, a layer of transparent TiO_2 paste (Dyesol, 18NR-T), both normal and protonated, was used. The photoanodes used were prepared following the same procedure reported in the previous section, and they were sensitized (5 h) using two different sensitizing baths: EtOH:THF (9:1) solutions of dyes in 0.2 mM concentration, with or without addition of 10.0 mM 3a,7a-dihydroxy-5b-cholic acid (CDCA). All the UV−vis absorption spectra were recorded using a Perkin-Elmer Lambda 800 spectrophotometer.

4. RESULTS AND DISCUSSION

4.1. Role of the Dye Molecular Structure and of the CB Position on Injection Rates. The results for all the investigated systems in the neutral monoprotonated form (hereafter termed 1H), starting with the Newns−Anderson analysis of the dye−TiO_2 complexes, are reported in Figure 4, where we also report the corresponding Lorentzian distribution and the PDOS relative to the semiconductor in the presence of the dye. Notice that the normalized dye's LUMO PDOS and the corresponding Lorentzian distributions have been multiplied by 50 and by the sensitizer's PDOS maximum value, respectively. The semiconductor's PDOS displays a profile that is practically the same as that of the corresponding DOS relative to the bare TiO_2 apart from a small upshift induced by the anchored sensitizer (see the CB edge energetic values for the isolated semiconductor (E_{CB}) and for the TiO_2 in the complex ($E_{CB\text{-}complex}$) in Table 1). These energy up-shifts, amounting to 0.1−0.2 eV, are the consequence of a combined effect of the electrostatic potential generated by the sensitizer (i.e., the dye dipole) on the TiO_2 surface and of the charge transferred by the dye to the TiO_2 by virtue of the dye−semiconductor chemical interaction.[19] Larger differences can be instead observed from the sensitizer side: when the dye is bound to the semiconductor, the LUMO tends to have significant contributions on a broad window of molecular orbitals, resulting in an energetic spread over a number of eigenvalues, as shown by the sizable broadenings exhibited by the dye's LUMO PDOS (green lines in Figure 4). We can, however, observe that the maximum of the sensitizer's LUMO distribution, for all the investigated systems, remains constantly at higher energies with respect to the CB edge of the TiO_2, as required for an efficient charge injection. Because of the choice of a standard deviation (σ = 0.3 eV) of the Gaussian functions used to represent the dye's PDOS, we cannot extract quantitative information about the broadening of the distribution and hence about the injection rates. To overcome this issue we resort to the Newns−Anderson model, which, as explained in the previous section, allows us to evaluate the energy of the LUMO for the adsorbed dye (eq 5) and the corresponding broadening (eq 6). Using this approach, one can also estimate the energetic shift of the dye's LUMO resulting from the adsorption on the semiconductor and its energetic Lorentzian distribution, represented by the blue lines in Figure 4.

Starting our discussion from the system containing the L0 dye (Figure 4a), we can observe that the sensitizer's LUMO PDOS is not symmetric because of considerable contributions at lower energies, responsible of the small shoulder at about −3.4 eV. This behavior produces a down-shift of the Lorentzian maximum with respect to that of the PDOS by 0.01 eV. The presence of significant dye contributions on a large number of complex eigenvalues implies a rather high estimated broadening amounting to 0.21 eV, which gives an electron injection time of about 3 fs. Despite the simplicity of the computational

dx.doi.org/10.1021/jp5004853 | J. Phys. Chem. C XXXX, XXX, XXX−XXX

strategy, as already discussed by Persson et al. in refs 84 and 94, the Newns−Anderson model is able to give reasonable estimations of the injection times, being in qualitative agreement with the theoretical and experimental reference data. In particular, our calculated value for the L0 dye is comparable with those evaluated by the use of different theoretical methods (2−10 fs, see refs 95 and 96), for similar organic sensitizers and is certainly <200 fs as expected from experimental measurements.[22,97]

Turning now to the JK2 dye, the plots in Figure 4b show that the sensitizer's LUMO PDOS distribution is centered at lower energies with respect to that of L0. In fact, while the L0 LUMO is energetically localized in the proximity of the semiconductor PDOS maximum, that of JK2 shows the major contributions in a region corresponding to the lower-energy profile of the TiO_2 states distribution. This behavior can be understood by simply considering that, even for the JK2 isolated dye, the LUMO energy is significantly lower (−3.00 eV) than that of the L0 sensitizer (−2.54 eV). In contrast to what was obtained for L0, the JK2 LUMO PDOS is almost symmetric, with a maximum coincident with that of the corresponding Lorentzian distribution. The significant differences observed in the LUMO PDOSs of the two analyzed dyes are clearly associated with relevant variations also in the broadenings of the sensitizer's state distributions. In particular we can notice that the JK2 adsorbed LUMO is mainly localized on the dye states than that of L0, as confirmed by the significantly lower value of the energetic broadening (0.14 eV), yielding a 40% increased electron injection time with respect to that computed for L0. Despite this, JK2 is in any case a dye showing good electron injection properties, as confirmed by the high efficiency (∼8%) obtained in cells built using this sensitizer.[71] Notice that also in this case the injection times are consistent with the reference data from the literature.[22,95−97] Providing an explanation for the differences observed in systems with apparently similar structure, i.e., same acceptor moiety, comparable donor group, and same anchoring geometry, is not straightforward. Jones et al.[95] motivated these effects by resorting to two properties strictly related to the molecular structure of the sensitizer, namely the electron injection energy (E_{LUMO}) and the percentage of LUMO localized on the anchoring moiety. The dependence of the injection rate on the LUMO energy, which essentially dictates the driving force and the coupling with the TiO_2 DOS, has been already widely discussed by several research groups.[98,99] We can attribute a part of the variations observed in the injection rates to the above-discussed shift between the LUMO energies of the two dyes in both the adsorbed and standalone forms. In particular, by a comparison of the Lorentzian distributions with the semiconductor PDOSs, we notice that L0 presents the LUMO in an energetic region where the TiO_2 states are more dense, while the JK2 LUMO is energetically localized close to the CB edge, where there are few semiconductor empty states available for the mixing. This effect can be approximately quantified by comparing the value of the TiO_2 DOS evaluated at the energy of the LUMO for the two systems. The calculated values reported in Table 1 for both the bare TiO_2 and the semiconductor in the presence of the sensitizer show that the L0 dye LUMO is located in an energetic region characterized by about 122 TiO_2 states/eV, a number significantly greater than the 89−96 states/eV found for the JK2 LUMO. Notice that these values can be used only for comparison purposes among different systems because of the dependence on the Gaussian broadening used to reproduce the semiconductor DOSs. The second aspect to be discussed here is the spatial localization of the dye's LUMO: we report in Figure 5 the isodensity plots of the LUMO for all the investigated isolated dyes in their protonated form at the geometry they have in the dye@TiO_2 complex. As expected from the shorter injection times, the LUMO of L0 has a higher contribution on the anchoring moiety with respect to that of JK2. The percentage of the LUMO on the anchoring moiety atoms can be obtained by summing the p_i contributions of the LUMO relative to the atoms of the cyanoacrylic group. A similar procedure can be applied also to the dye adsorbed on the semiconductor by performing the sum on a number of complex states containing a unitary contribution of the sensitizer. As expected, we found that L0, in its free protonated form, has about 31% of the LUMO localized in the anchoring moiety while for JK2 this state is more distributed along the molecule and shows a percentage of 24% on the cyanoacrylic group; if we consider the dyes in the complex with the TiO_2, the two percentages tend to increase because of the dye interaction with the surface Ti(IV) atoms, but a comparable difference between the two systems still remains (66% for L0 and 51% for JK2).

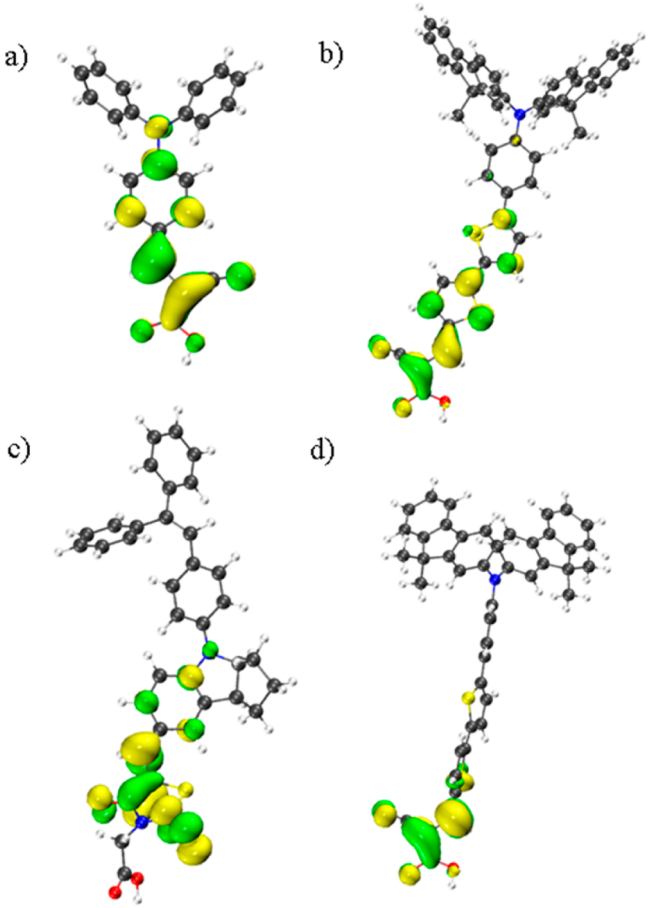

Figure 5. Isodensity surfaces of the LUMO for the L0 (a), JK2 (b), D102 (c), and JK2-T (d) dyes. Green (yellow) areas correspond to positive (negative) regions of the orbital. The orbital value at the surface is ±0.04.

To further elucidate the effect of the spatial localization of the LUMO, we investigated, for the system containing the JK2 dye, how the breaking of the electron conjugation can influence the injection rate by simply twisting by 90° the C−C bond connecting the cyanoacrylic anchoring moiety to the first

dx.doi.org/10.1021/jp5004853 | J. Phys. Chem. C XXXX, XXX, XXX−XXX

thiophene ring of the π-spacer; the corresponding PDOSs are reported in Figure 4c. It is worth noting that while the dye's LUMO energy is almost unaffected by the twisting of the bond (the energy change is only 0.05 eV), the broadening of the LUMO distribution is strongly modified (Figure 4c). By the analysis of the corresponding Lorentzian distribution, we quantified the increase in the broadening, amounting to about 0.07 eV. From these values we then evaluated the injection time for the JK2-T dye, obtaining a value of 3 fs. As the breaking of the conjugation has a negligible effect on the LUMO energy, this large increase in the injection rate can be completely attributed to the increase of the LUMO localization on the anchoring region. As a matter of fact, passing from the planar to the twisted JK2 configuration, the LUMO localization on the cyanoacrylic moiety increases by about 18% and 35% in dye in its free and adsorbed form, respectively (Figure 5).

We conclude this analysis by discussing the case of the D102 dye, which is attached to TiO_2 by a nonconjugated rhodanine-3-acetic anchoring moiety[10] (Figure 2b). The effects on the injection and recombination rates generated by the substitution of the cyanoacrylic group with the rhodanine units have already been discussed in ref 41. The data relative to D102 are plotted in Figure 4d, where we notice that the LUMO PDOS maximum is energetically localized at higher energies with respect to that of the other dyes, as confirmed by the adsorbed LUMO position at −2.68 eV. As expected, we also calculate a small stabilization (0.07 eV) of the lowest-energy unoccupied state between the free (−2.61 eV) and adsorbed system, which clearly suggests a small coupling between the sensitizer and the semiconductor states. A preliminary confirmation of this effect can be found in the small energetic broadening found for this system (0.12 eV), yielding an increased injection time, ∼ 6 fs. As shown in Figure 5c, the LUMO component on the carboxylic unit is negligible, as confirmed by the practically zero percentage of the first unoccupied orbital on the anchoring moiety. For D102 anchored on TiO_2, the LUMO localization on the carboxylic group slightly increases although it remains consistently lower (12%) than those relative to the other dyes (L0@TiO_2, 22%; JK2@TiO_2, 17%; JK2-T@TiO_2, 26%). Despite this very low localization of the injecting orbital on the anchoring unit, the charge-transfer rate, as seen above, remains in the ultrafast timescale (<100 fs). These relatively fast injection kinetics can be explained considering the LUMO energetic position, localized in a dense region of TiO_2 states (∼126 states/eV for the bare semiconductor and ∼130 states/eV for the TiO_2 in the presence of the sensitizer, Table 1).

4.2. TiO_2 Protonation: Energy Level Shifts and Dye−Semiconductor Electronic Coupling. As discussed in the Introduction, the TiO_2 CB position can be effectively tuned by varying the pH: raising the proton concentration results in a stabilization of the CB edge.

The effects on the TiO_2 DOS relative to the unoccupied states as the number of protons on the surface increases is shown in Figure 6. As expected, by adsorbing protons to the bare TiO_2 cluster, the DOS profile tends to linearly decrease in energy, yielding a constant CB edge shift. Data in Figure 6 follow a perfectly linear trend ($R^2 = 0.99$), and from the slope of the fitted line we can precisely quantify the CB energetic shift due to the addition of a single proton (or a general positive charge) on the TiO_2 surface amounting to about 0.1 eV.

Turning now to the dye-sensitized TiO_2, the following question arises: How does TiO_2 protonation modify the relative dye/semiconductor energy level alignment and the electronic coupling? Similar to what we have previously shown for the cationic additives in the D102-sensitized TiO_2 film,[62] the effect on the injection rates upon surface protonation can be basically attributed to two interplaying factors: (i) the dependence of the TiO_2 DOS and of the dye's LUMO position on the number of H^+ adsorbed on the surface and (ii) the variation of the coupling matrix elements between the sensitizer and the semiconductor. Here we go beyond the Newns−Anderson model by moving to a diabatic-like description of the problem based on the localization of the interacting complex orbitals on the donor (sensitizer) and acceptor (TiO_2) species, giving us explicit information on the electronic coupling between the sensitizer and the semiconductor.

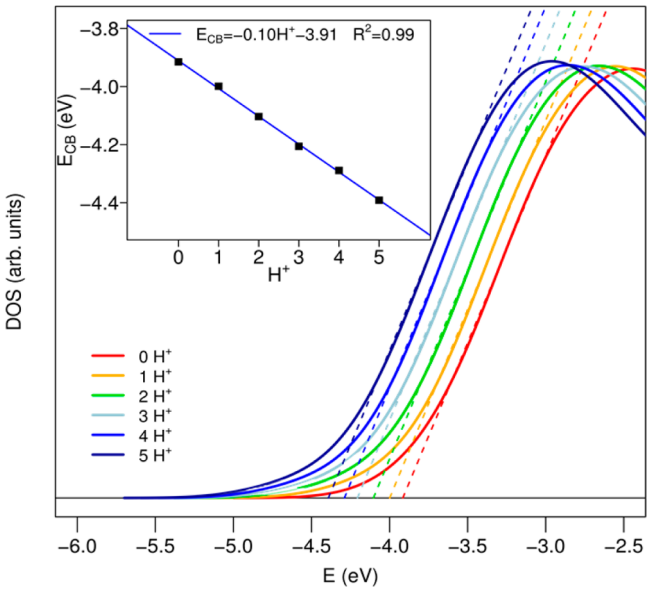

Figure 6. Effect of protons on the TiO_2 DOS (main panel) and on the energy of the CB edge (inset).

The results for the L0@TiO_2 system in all the modeled protonation forms (from 1H to 5H) are reported in Figure 7, while those for the JK2 and D102 dyes in both 1H and 5H forms investigated are displayed in Figure 8. We plot the modulus of the electronic coupling matrix elements between the dye LUMO and a wide range of TiO_2 virtual state as a function of the energy. Together with the coupling elements, we plot the injection function, $\Gamma(E)$, evaluated in electronvolts by means of $\Gamma = \hbar k_{inj}$ and the density of the unoccupied complex states localized on the TiO_2 cluster. Then, in Table 2 we collect some relevant quantities extracted upon the diabatization step: the energy of the diabatic TiO_2 CB; the dye's HOMO and LUMO, with the associated HOMO−LUMO gap; and the injection function $\Gamma(E)$ evaluated at the energy of both diabatic and Lorentzian (NA) LUMO, which is also reported for the sake of completeness.

Let us start by discussing the case of L0: as is apparent from the plots in Figure 7, the larger coupling elements are those corresponding to the lower-energy TiO_2 unoccupied states, with values reaching about 0.10 eV for the monoprotonated case and exceeding 0.12 eV in the 5H form. Overall, we observe a very regular trend as the number of protons on the surface increases, with the only exception being the 2H case, which shows an exaggerated increment of the electronic coupling in the low-energy region, possibly due to the fact that the only positive charge is located at one of the cluster corners. As higher energies

dx.doi.org/10.1021/jp5004853 | J. Phys. Chem. C XXXX, XXX, XXX−XXX

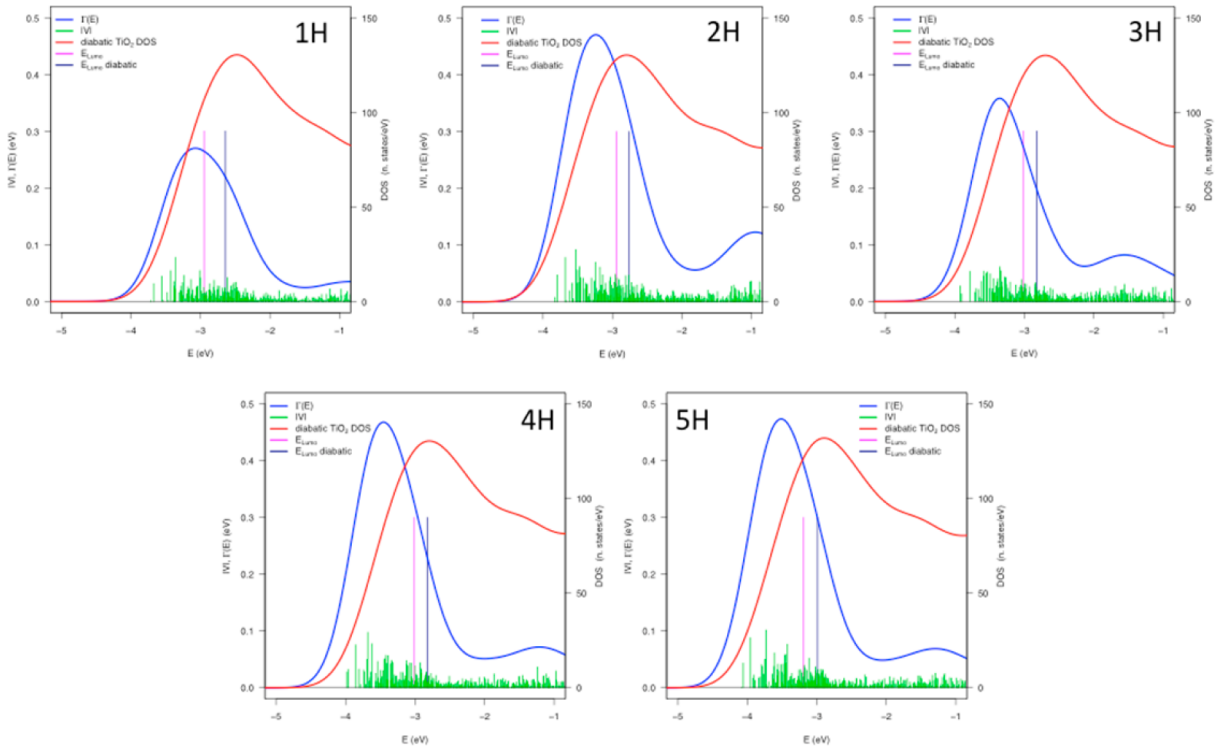

Figure 7. Absolute value of the coupling matrix elements (V_{dk}) between the dye LUMO and the TiO_2 virtual states (green sticks), injection broadening $\Gamma(E)$ function (blue line), and DOS relative to the virtual localized (diabatic) orbital of the semiconductor (red line) for L0@TiO_2 in different protonation forms as a function of the energy (E). For each system the magenta and blue vertical lines represent the energetic position of the adsorbed dye LUMOs evaluated as the maximum of the Newns−Anderson Lorentzian distribution and as the energy of the localized orbital more similar to the sensitizer's first virtual state, respectively. The Gaussian broadening used to reproduce both the TiO_2 DOS and the $\Gamma(E)$ function is equal to 0.3 eV.

are considered, the coupling values progressively tend to decrease. Small deviations from this trend can be observed only in the dye LUMO energetic region where the coupling matrix elements tend slightly to rise because of the extreme proximity (in energy terms) of the interested TiO_2 states with respect to the donor orbital. As a consequence, the corresponding $\Gamma(E)$ function shows a pronounced maximum in correspondence of the TiO_2 CB edge region. The progressive increasing of the protonation degree yields a sizable energetic shift of the Γ distribution maximum, which is clearly related to semiconductor CB edge lowering discussed above and displayed in Figure 6. The linear dependence of Γ on the TiO_2 DOS can be easily verified by observing the great similarity in the down-shift of the injection rate maximum (0.44 eV) with respect to that of the CB edge energetic position (about 0.40 eV) between the two extreme protonation forms (1H and 5H). As we have already mentioned above, the intensity of the Γ function seems instead to follow only the coupling energetic trend. This clearly implies significantly higher injection rates for the 5H form (0.47 eV at the maximum position) with respect to the monoprotonated form (0.27 eV at the same energetic position), in particular in the energetic regions closer to the maximum of the distribution. A confirmation of this phenomenon can be found in the very similar TiO_2 DOS values extracted at the Γ maximum energetic position for the two protonated form (93 states/eV for the 1H and 89 states/eV for the 5H).

By extracting the value of $\Gamma(E)$ at the sensitizer's LUMO energy, one can estimate the charge injection rate from the dye to the semiconductor. It is worthwhile to stress that the position of the dye LUMO can be evaluated in two different ways: in the adiabatic picture, as the energy of the Newns−Anderson Lorentzian distribution maximum ($LUMO_{NA}$, magenta sticks in Figures 7 and 8) and, in the diabatic framework, as the energy of the localized orbital corresponding to the dye LUMO (dark blue sticks in Figures 7 and 8). Although the two methods give slightly different results, with the Lorentzian distribution energetic position always more stabilized than the LUMO orbital obtained by the diabatization, the variations remain sufficiently small. It is worthwhile to highlight, however, that such a small difference delivers negligible variations in the estimated Γ values (within 0.01−0.09 eV). In light of these considerations, we then extracted the Γ function intensity in the dye LUMO range, obtaining a value of about 0.22−0.25 eV (corresponding to about 3 fs) for the 1H form and 0.30−0.39 eV (~2 fs) for the 5H case. Similar conclusions can be drawn also for the system containing the JK2 dye (upper panels in Figure 8). Also in this case the addition of an increasing number of protons on the TiO_2 surface produces an increase in the coupling matrix elements, again in the lower-energy region. Comparing the $\Gamma(E)$ curves with those of the L0 dye, we can immediately notice a lowering of the injection rates (about 0.1 eV at the maxima energetic position) in the whole energy range and for both the protonation, imputable to the smaller spatial localization of the LUMO on the anchoring unit found in JK2 compared to L0. This trend is consistent with the results provided by the Newns−Anderson model and discussed in the previous section. However, by extracting the $\Gamma(E)$ function in the dye LUMO range, we obtain injection rate values of 0.23 eV for the 1H form and 0.37−0.40 eV for the 5H case, which result in values somewhat larger than those calculated for the corresponding L0 systems. This is clearly the result of a more favorable energetic position of the dye's LUMO, which, lying at lower energies, can inject into the CB states for which the

dx.doi.org/10.1021/jp5004853 | J. Phys. Chem. C XXXX, XXX, XXX−XXX

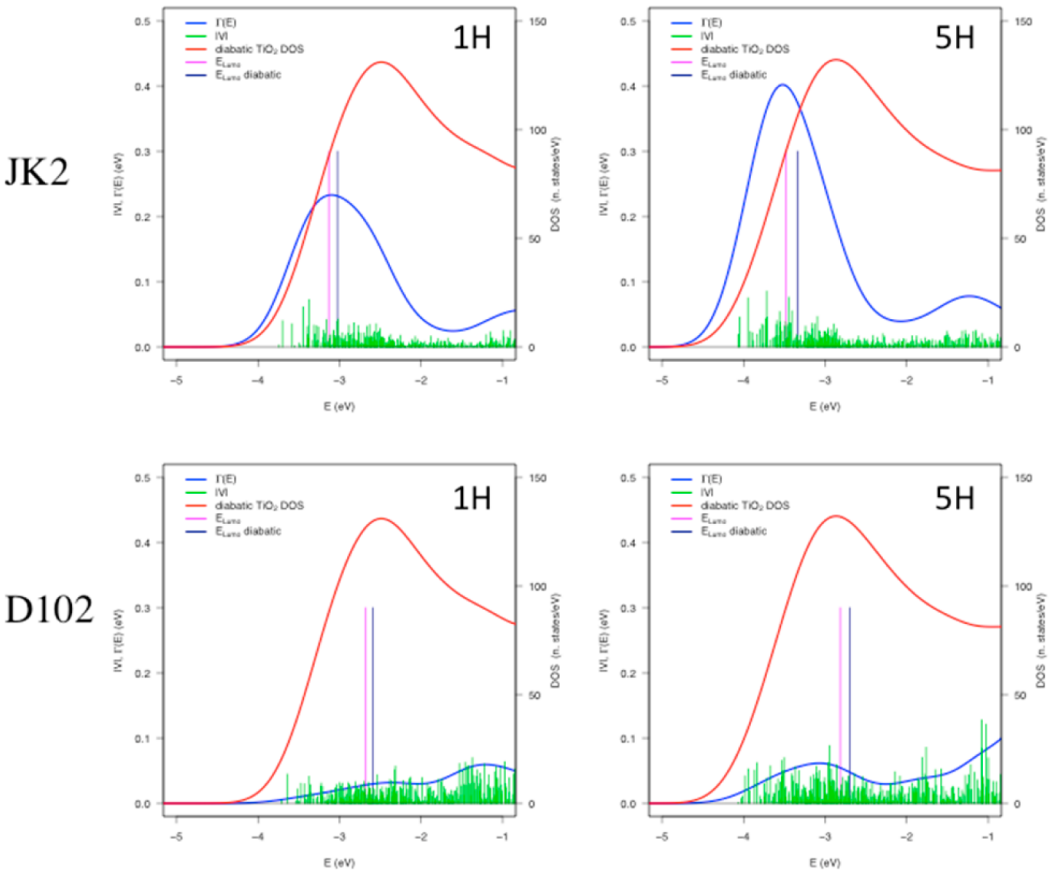

Figure 8. Absolute value of the coupling matrix elements (V_{dk}) between the dye LUMO and the TiO_2 virtual states (green sticks), injection broadening $\Gamma(E)$ function (blue line), and DOS relative to the virtual localized (diabatic) orbital of the semiconductor (red line) for the JK2@TiO_2 and D102@TiO_2 systems in the 1H (left panels) and 5H (right panels) protonation form as a function of the energy (E). For each system, the magenta and blue vertical lines represent the energetic position of the adsorbed dye LUMOs evaluated as the maximum of the Newns−Anderson Lorentzian distribution and as the energy of the localized orbital more similar to the sensitizer first virtual state, respectively. The Gaussian broadening used to reproduce both the TiO_2 DOS and the $\Gamma(E)$ function is equal to 0.3 eV. Note that in the case of the D102 dye (bottom panels) both the coupling matrix elements (V_{dk}) and the $\Gamma(E)$ function were multiplied by 10.

Table 2. Calculated Energies (Electronvolts) of Diabatic TiO_2 Conduction Band (CB_{DIA}), Dye's HOMO and LUMO and HOMO−LUMO Gap (GAP_{DIA}), Injection Function ($\Gamma(E)$) Evaluated at the Energy of Both Diabatic (Γ^{DIA}, $LUMO_{DIA}$) and Lorentzian (Γ^{DIA}, $LUMO_{NA}$) LUMO, and Lorentzian LUMO ($LUMO_{NA}$)

proton no.	CB_{DIA}	$LUMO_{DIA}$	$HOMO_{DIA}$	GAP_{DIA}	Γ^{DIA} ($LUMO_{DIA}$)	$LUMO_{NA}$	Γ^{DIA} ($LUMO_{NA}$)
				L0			
1H	−3.830	−2.643	−5.603	2.959	0.220	−2.793	0.247
2H	−4.132	−2.762	−5.685	2.923	0.327	−2.945	0.410
3H	−4.042	−2.826	−5.721	2.895	0.199	−3.012	0.271
4H	−4.132	−2.921	−5.783	2.862	0.279	−3.120	0.377
5H	−4.229	−2.991	−5.836	2.845	0.302	−3.190	0.392
				JK2			
1H	−3.846	−3.025	−5.100	2.074	0.231	−3.131	0.233
5H	−4.220	−3.337	−5.214	1.877	0.375	−3.484	0.401
				D102			
1H	−3.999	−2.593	−5.188	2.596	0.003	−2.683	0.003
5H	−4.391	−2.699	−5.188	2.489	0.005	−2.815	0.006

electronic coupling is higher (i.e., the LUMO position falls in the region where the $\Gamma(E)$ function shows the maximum).

Turning now to the nonconjugated D102 dye, comparing the injection rates in Table 2 with those reported in Table 1, we observe a substantial disagreement between the results provided by the two approaches. In fact, by considering the explicit coupling between the LUMO and the CB states, we obtain injection rates of 0.003 (1H) and 0.005 eV (5H), whereas the values obtained by the Lorentzian broadening are 0.12 (1H) and 0.16 eV (5H). While the diabatic results are clearly consistent with the not conjugated structure of the dye and with the negligible localization of the dye's LUMO on the carboxylate anchoring group, the broadening estimated in the Newns−Anderson model by means of a Mulliken population analysis is

dx.doi.org/10.1021/jp5004853 | J. Phys. Chem. C XXXX, XXX, XXX−XXX

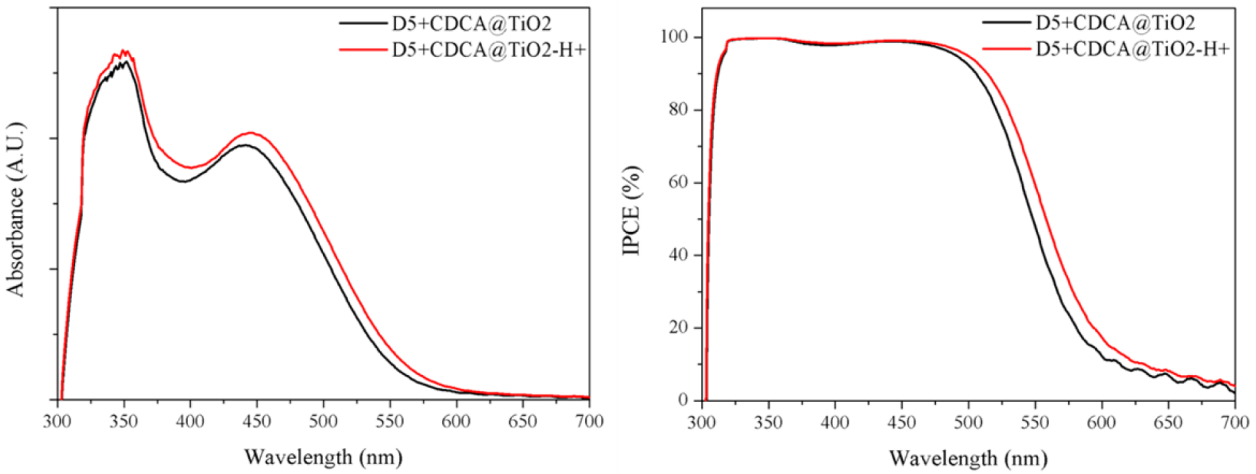

Figure 9. Left panel: UV−vis absorption spectra of D5 with CDCA adsorbed both on titania (black line) and on protonated titania (red line). Right panel: calculated IPCE obtained from UV−vis absorption spectra of D5-sensitized titania layer (left panel).

evidently sensitive to the basis set quality choice, a well-know drawback of this kind of electron population scheme, where the electron density is projected onto the basis set.[100]

Interestingly, comparing the CB and LUMO energy levels for the different dyes, reported in Table 2, one can notice that while the extent of the CB_{DIA} down-shift as the number of protons increases does not depend on the particular dye adsorbed, different dyes show different down-shifts of the LUMO going from the 1H to 5H forms. While the stabilization of the LUMO (both diabatic and NA) is in the range 0.35−0.39 eV, comparable to the ca. 0.40 eV shift of the CB edge, we observe a sizeably smaller stabilization of the D102 LUMO, amounting to about 0.1 eV. This is clearly the consequence of the different electronic structure of the interface: the energy levels of the conjugated dyes (L0 and JK2) are more strongly perturbed by the surface protonation, and the stabilization of the TiO_2 CB edge translates into a similar stabilization of the dye's LUMO, while the LUMO of the uncoupled D102 dye is practically unaffected by what happens to the TiO_2 DOS. As a consequence of the progressive charge accumulation on the surface, also the dye's HOMO turns out to be stabilized in the case of the conjugated dyes: in the shorter L0 system, where the ground-state electronic charge can be more effectively transferred to the protonated TiO_2,[19] the down-shift amounts to 0.23 eV, whereas in the longer JK2 dye, the HOMO stabilization is about 0.1 eV. For the same reasons, the D102 HOMO is practically unchanged upon TiO_2 protonation. The different HOMO and LUMO energy shifts with surface protonation lead to an overall reduction of the dye's HOMO−LUMO gap (see Table 2) with an increase in the number of adsorbed protons. The entity of such HOMO−LUMO gap variation is strongly dependent on the electronic structure of the dye, and it is fully in line with the observed red-shift of the absorption spectrum of D5-sensitized TiO_2 upon acidic treatment, which was recently reported by some of us.[67] To better rationalize the relation between the predicted change in the optical properties of the protonated dye-sensitized TiO_2 film,[66] the calculated enhanced injection rates, and the measured photocurrents and device efficiencies, we report in the next section a spectroscopic and photovoltaic study of protonated and not protonated sensitized TiO_2 films employing the prototypical D5 organic dye.

4.3. TiO_2 Protonation: Spectroscopic and Photovoltaic Study. In Figure 9, the UV−vis absorption spectra and the corresponding IPCE curves of D5+CDCA@TiO_2 for both protonated and not protonated cases are reported. For the D5+CDCA@TiO_2, the recorded absorption spectrum shows a maximum at 441 nm, in good agreement with the 444 nm absorption peak reported in the literature;[101] moving to protonated TiO_2, as computationally predicted, see Table 2, the absorption maximum slightly shifts at longer wavelengths, appearing at 446 nm. The spectra of Figure 9 also show that the substrate protonation yields the expected enhancement in the absorbance arising from an increase in the dye loading, which has been reported in the literature.[60,102]

Figure 10 displays the $J-V$ curves of the best-performing devices, while the photovoltaic data of all devices are collected in Table 3.

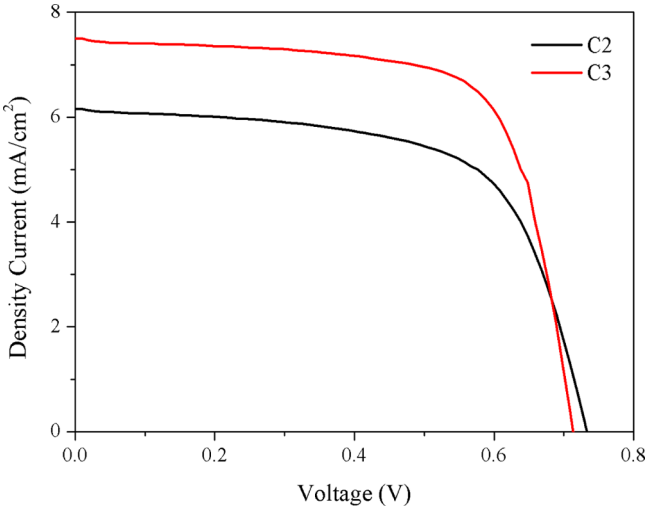

Figure 10. $J-V$ curves of the highest-efficiency devices, without (C2) and with (C3) acidic treatment of the TiO_2.

As it is apparent from the photovoltaic data above, the photoanode protonation (C3 and C4 cells) leads to a significant improvement in the measured photocurrent density compared to that of untreated photoanodes (C1 and C2 cells), while the open circuit voltages slightly decrease, in line with the results of previously published works.[46,54] The subtle variations observed in the FF values for cells built under the same conditions are

dx.doi.org/10.1021/jp5004853 | J. Phys. Chem. C XXXX, XXX, XXX−XXX

Table 3. Photovoltaic Data of D5-Based Devices

cell	acidic treatment	Jsc (mA/cm^2)	V_{oc} (V)	FF	eff. (%)
C1	no	5.780	0.734	0.688	2.92
C2	no	6.150	0.734	0.636	2.87
C3	yes	7.500	0.713	0.699	3.74
C4	yes	6.453	0.724	0.647	3.02

probably due to unavoidable fluctuations in the reproducibility of the device fabrication procedure. On the basis of the experimental results alone, the measured higher photocurrent values might be rationalized as arising from the spectral modifications shown in Figure 9 (left panel), namely, (i) an increased absorbance and (ii) an extension of the absorption spectral window due to the spectral red-shift. On the other hand, the results of our theoretical analysis clearly show that the presence of protons on the titania surface always translates into higher electronic coupling and injection rates and hence possibly into higher photocurrents, under the assumption that the recombination losses are not affected by the substrate protonation. Here, to disentangle the effects of the spectral red-shift and the improved interfacial charge separation on the measured photocurrents, we have calculated the maximum gain in J_{sc} caused by the improved spectral properties. First of all, from the D5-sensitized-protonated-TiO_2 absorption spectra (Figure 99, left panel), we have obtained the "theoretical" IPCE (reported in Figure 9, right panel). We recall that IPCE = LHE $\times \phi_{INJ} \times \phi_{COLL}$, where LHE is the light harvesting efficiency of the photoelectrode, ϕ_{INJ} is the quantum yield of electron injection and ϕ_{COLL} is the electron collection efficiency at the TCO. In order to quantify the effect on the IPCE only due to the spectral modifications we consider both ϕ_{INJ} and ϕ_{COLL} equal to 1 and consequently approximate the IPCE as follows

$$\text{IPCE} \approx \text{LHE} = 1 - 10^{A} \tag{8}$$

where A is the absorbance of D5-sensitized-protonated-TiO_2 absorption spectrum. Then we obtained J_{sc} from the calculated IPCE (Figure 9, right panel and eq 8) by applying the equation

$$J_{SC}\ (\text{mA/cm}^2) = \int \frac{P_{in} \times \lambda}{1.99 \times 10^{-16}} \times \frac{\text{IPCE}_{\lambda}}{100} \times \frac{1}{6.24 \times 10^{18}} \tag{9}$$

where P_{in} is the incident power of solar spectrum and IPCE_{λ} is, for our case, the IPCE calculated with eq 8. By comparing the photocurrent densities obtained from eq 9, we found that the maximum photocurrent gain imputable to the spectral red-shift and increased absorbance of the protonated titania, should be about 0.7 mA/cm^2; this value is considerably lower than the increment found in the measured photocurrents (see Table 3), amounting to about 1.4 mA/cm^2. These findings, in agreement with the theoretically predicted higher electronic coupling and injection rates, confirm that in addition to the augmented dye loading and the spectral red-shift, which might yield higher photocurrent values, the surface protonation increases the interfacial electronic coupling between the dye and the semiconductor, overall improving the charge-separation and charge-injection processes.

5. CONCLUSIONS

In this paper we have presented a joint theoretical and experimental investigation on the effect of TiO_2 protonation on the interfacial electronic coupling and injection rates and also in relation to the different molecular structure of the dye (length of conjugation, conjugated vs not-conjugated anchoring group). The dependence of the injection rate on the dye molecular structure has been investigated here by the Newns–Anderson model, comparing different sensitizers as well as various configurations of the same dye, with the aim of elucidating the effects of the breaking of the electron conjugation. In line with available experimental and theoretical data, we found that changes in the units constituting the sensitizer (without altering the conjugation) produces variations both on the energy and on the spatial localization of the injecting orbital (in our case the LUMO), which clearly reflects on the energetic alignment between the dye and TiO_2 states and on the coupling between the interacting species, with inevitable consequences on the corresponding injection rates. The breaking of the electron conjugation, on the other side, principally reflects on the localization of the injecting orbital on the anchoring moiety, with a drastic increment in the coupling between the dye states and the TiO_2 CB.

We then investigated the effects produced by a shift of the TiO_2 CB edge, simulated by adsorbing an increasing number of protons (from 0 to 5) on the semiconductor surface, on the calculated injection rates. This analysis was performed by making use of a diabatic-like treatment, which provided us with the coupling matrix elements between the injecting orbital (dye's LUMO) and the semiconductor CB acceptor states. We have clearly demonstrated that the addition of protons on the semiconductor surface, while producing a consistent shift of both the TiO_2 CB and dye LUMO energetic positions, influences the injection rate mainly through the variations generated in the coupling matrix elements, in particular with the semiconductor states in the lower-energy region. Employing the prototypical D5 dye, we then experimentally verified the predicted spectral red-shift with increasing TiO_2 protonation and evaluated the impact of TiO_2 protonation on the DSCs photovoltaic characteristics. On the one hand, the substrate protonation produces a slight red-shift of the absorption spectrum associated to an increased absorbance;[67] on the other hand, we have shown that the measured increase in the generated photocurrent cannot be solely due to the above-mentioned spectral modifications.

The present contribution represents, in our opinion, an advance toward an even deeper comprehension of the various factors governing the optical properties and charge-separation processes occurring at the liquid/solid dye/TiO_2 interface in working DSC devices, showing how the environmental effects separately influence the energetics, optical properties, and electronic structure of the interface.

AUTHOR INFORMATION

Corresponding Authors

*M.P: e-mail, chiara@thch.unipg.it.

*F.D.A.: e-mail, filippo@thch.unipg.it.

Notes

The authors declare no competing financial interest.

ACKNOWLEDGMENTS

The authors thank FP7-ENERGY-2010 project ESCORT (261920) and CNR-EFOR for financial support.

REFERENCES

(1) O'Regan, B.; Grätzel, M. A Low-Cost, High-Efficiency Solar Cell Based on Dye-Sensitized Colloidal TiO_2 Films. *Nature* **1991**, *353*, 737–740.

(2) Nazeeruddin, M. K.; De Angelis, F.; Fantacci, S.; Selloni, A.; Viscardi, G.; Liska, P.; Ito, S.; Takeru, B.; Grätzel, M. Combined Experimental and DFT-TDDFT Computational Study of Photoelectrochemical Cell Ruthenium Sensitizers. *J. Am. Chem. Soc.* **2005**, *127*, 16835−16847.
(3) Nazeeruddin, M. K.; Bessho, T.; Cevey, L.; Ito, S.; Klein, C.; De Angelis, F.; Fantacci, S.; Comte, P.; Liska, P.; Imai, H.; et al. A High Molar Extinction Coefficient Charge Transfer Sensitizer and Its Application in Dye-Sensitized Solar Cell. *J. Photochem. Photobiol., A* **2007**, *185*, 331−337.
(4) Hagfeldt, A.; Peter, L. *Dye-sensitized Solar Cells*: EPFL Press: Lausanne, 2010.
(5) Han, L.; Islam, A.; Chen, H.; Malapaka, C.; Chiranjeevi, B.; Zhang, S.; Yang, X.; Yanagida, M. High-Efficiency Dye-Sensitized Solar Cell with a Novel Co-Adsorbent. *Energy Environ. Sci.* **2012**, *5*, 6057−6060.
(6) Yella, A.; Lee, H.-W.; Tsao, H. N.; Yi, C.; Chandiran, A. K.; Nazeeruddin, M. K.; Diau, E. W.-G.; Yeh, C.-Y.; Zakeeruddin, S. M.; Grätzel, M. Porphyrin-Sensitized Solar Cells with Cobalt (II/III)−Based Redox Electrolyte Exceed 12 Percent Efficiency. *Science* **2011**, *334*, 629−634.
(7) Hagberg, D. P.; Marinado, T.; Karlsson, K. M.; Nonomura, K.; Qin, P.; Boschloo, G.; Brinck, T.; Hagfeldt, A.; Sun, L. Tuning the HOMO and LUMO Energy Levels of Organic Chromophores for Dye Sensitized Solar Cells. *J. Org. Chem.* **2007**, *72*, 9550−9556.
(8) Grätzel, M. Recent Advances in Sensitized Mesoscopic Solar Cells. *Acc. Chem. Res.* **2009**, *42*, 1788−1798.
(9) Mishra, A.; Fischer, M. K. R.; Bäuerle, P. Metal-Free Organic Dyes for Dye-Sensitized Solar Cells: From Structure:Property Relationships to Design Rules. *Angew. Chem., Int. Ed.* **2009**, *48*, 2474−2499.
(10) Pastore, M.; De Angelis, F. Aggregation of Organic Dyes on TiO_2 in Dye-Sensitized Solar Cells Models: An ab Initio Investigation. *ACS Nano* **2010**, *4*, 556−562.
(11) Pastore, M.; Mosconi, E.; De Angelis, F.; Grätzel, M. A Computational Investigation of Organic Dyes for Dye-Sensitized Solar Cells: Benchmark, Strategies, and Open Issues. *J. Phys. Chem. C* **2010**, *114*, 7205−7212.
(12) Ito, S.; Zakeeruddin, S. M.; Humphry-Baker, R.; Liska, P.; Charvet, R.; Comte, P.; Nazeeruddin, M. K.; Péchy, P.; Takata, M.; Miura, H.; et al. High-Efficiency Organic-Dye-Sensitized Solar Cells Controlled by Nanocrystalline-TiO_2 Electrode Thickness. *Adv. Mater.* **2006**, *18*, 1202−1205.
(13) Ito, S.; Miura, H.; Uchida, S.; Takata, M.; Sumioka, K.; Liska, P.; Comte, P.; Pechy, P.; Grätzel, M. High-Conversion-Efficiency Organic Dye-Sensitized Solar Cells with a Novel Indoline Dye. *Chem. Commun.* **2008**, 5194−5196.
(14) Zhang, G.; Bala, H.; Cheng, Y.; Shi, D.; Lv, X.; Yu, Q.; Wang, P. High Efficiency and Stable Dye-Sensitized Solar Cells with an Organic Chromophore Featuring a Binary π-Conjugated Spacer. *Chem. Commun.* **2009**, 2198−2200.
(15) Yum, J.-H.; Baranoff, E.; Kessler, F.; Moehl, T.; Ahmad, S.; Bessho, T.; Marchioro, A.; Ghadiri, E.; Moser, J.-E.; Yi, C.; et al. A Cobalt Complex Redox Shuttle for Dye-Sensitized Solar Cells with High Open-Circuit Potentials. *Nat. Commun.* **2011**, *3*, 631.
(16) Mosconi, E.; Yum, J.-H.; Kessler, F.; García, C. J. G.; Zuccaccia, C.; Cinti, A.; Nazeeruddin, M. K.; Grätzel, M.; De Angelis, F. Cobalt Electrolyte/Dye Interactions in Dye-Sensitized Solar Cells: A Combined Computational and Experimental Study. *J. Am. Chem. Soc.* **2012**, *134*, 19438−19453.
(17) Daeneke, T.; Kwon, T.-H.; Holmes, A. B.; Duffy, N. W.; Bach, U.; Spiccia, L. High-Efficiency Dye-Sensitized Solar Cells with Ferrocene-Based Electrolytes. *Nat. Chem.* **2011**, *3*, 211−215.
(18) Feldt, S. M.; Gibson, E. A.; Gabrielsson, E.; Sun, L.; Boschloo, G.; Hagfeldt, A. Design of Organic Dyes and Cobalt Polypyridine Redox Mediators for High-Efficiency Dye-Sensitized Solar Cells. *J. Am. Chem. Soc.* **2010**, *132*, 16714−16724.
(19) Ronca, E.; Pastore, M.; Belpassi, L.; Tarantelli, F.; De Angelis, F. Influence of the Dye Molecular Structure on the TiO_2 Conduction Band in Dye-Sensitized Solar Cells: Disentangling Charge Transfer and Electrostatic effects. *Energy Environ. Sci.* **2013**, *6*, 183−193.
(20) Liu, J.; Li, R.; Si, X.; Zhou, D.; Shi, Y.; Wang, Y.; Jing, X.; Wang, P. Oligothiophene Dye-Sensitized Solar Cells. *Energy Environ. Sci.* **2010**, *3*, 1924−1928.
(21) Miyashita, M.; Sunahara, K.; Nishikawa, T.; Uemura, Y.; Koumura, N.; Hara, K.; Mori, A.; Abe, T.; Suzuki, E.; Mori, S. Interfacial Electron-Transfer Kinetics in Metal-Free Organic Dye-Sensitized Solar Cells: Combined Effects of Molecular Structure of Dyes and Electrolytes. *J. Am. Chem. Soc.* **2008**, *130*, 17874−17881.
(22) Wiberg, J.; Marinado, T.; Hagberg, D. P.; Sun, L.; Hagfeldt, A.; Albinsson, B. Effect of Anchoring Group on Electron Injection and Recombination Dynamics in Organic Dye-Sensitized Solar Cells. *J. Phys. Chem. C* **2009**, *113*, 3881−3886.
(23) Rühle, S.; Greenshtein, M.; Chen, S. G.; Merson, A.; Pizem, H.; Sukenik, C. S.; Cahen, D.; Zaban, A. Molecular Adjustment of the Electronic Properties of Nanoporous Electrodes in Dye-Sensitized Solar Cells. *J. Phys. Chem. B* **2005**, *109*, 18907−18913.
(24) De Angelis, F.; Fantacci, S.; Selloni, A.; Grätzel, M.; Nazeeruddin, M. K. Influence of the Sensitizer Adsorption Mode on the Open-Circuit Potential of Dye-Sensitized Solar Cells. *Nano Lett.* **2007**, *7*, 3189−3195.
(25) Gao, Y. Q.; Marcus, R. A. On the Theory of Electron Transfer Reactions at Semiconductor/Liquid Interfaces. II. A Free Electron Model. *J. Chem. Phys.* **2000**, *113*, 6351−6360.
(26) Moser, J. E.; Grätzel, M. Observation of Temperature Independent Heterogeneous Electron Transfer Reactions in the Inverted Marcus Region. *Chem. Phys.* **1993**, *176*, 493−500.
(27) Hagfeldt, A.; Grätzel, M. Light-Induced Redox Reactions in Nanocrystalline Systems. *Chem. Rev.* **1995**, *95*, 49−68.
(28) Rehm, J. M.; McLendon, G. L.; Nagasawa, Y.; Yoshihara, K.; Moser, J.; Grätzel, M. Femtosecond Electron-Transfer Dynamics at a Sensitizing Dye−Semiconductor (TiO_2) Interface. *J. Phys. Chem.* **1996**, *100*, 9577−9578.
(29) Huber, R.; Moser, J.-E.; Grätzel, M.; Wachtveitl, J. Real-Time Observation of Photoinduced Adiabatic Electron Transfer in Strongly Coupled Dye/Semiconductor Colloidal Systems with a 6 fs Time Constant. *J. Phys. Chem. B* **2002**, *106*, 6494−6499.
(30) Schnadt, J.; Brühwiler, P. A.; Patthey, L.; O'Shea, J. N.; Södergren, S.; Odelius, M.; Ahuja, R.; Karis, O.; Bässler, M.; Persson, P.; et al. Experimental Evidence for sub-3-fs Charge Transfer from an Aromatic Adsorbate to a Semiconductor. *Nature* **2002**, *418*, 620−623.
(31) Huber, R.; Moser, J. E.; Grätzel, M.; Wachtveitl, J. Observation of Photoinduced Electron Transfer in Dye/Semiconductor Colloidal Systems with Different Coupling Strengths. *Chem. Phys.* **2002**, *285*, 39−45.
(32) Gerischer, H.; Willig, F. Reaction of Excited Dye Molecules at Electrodes. *Top. Curr. Chem.* **1976**, *61*, 31−84.
(33) Gerischer, H. Electrochemical Techniques for the Study of Photosensitization. *Photochem. Photobiol.* **1972**, *16*, 243−260.
(34) Marcus, R. A. On the Theory of Electron-Transfer Reactions. VI. Unified Treatment for Homogeneous and Electrode Reactions. *J. Chem. Phys.* **1965**, *43*, 679−701.
(35) Ardo, S.; Meyer, G. J. Photodriven Heterogeneous Charge Transfer with Transition-Metal Compounds Anchored to TiO_2 Semiconductor Surfaces. *Chem. Soc. Rev.* **2009**, *38*, 115−164.
(36) Listorti, A.; Creager, C.; Sommeling, P.; Kroon, J.; Palomares, E.; Fornelli, A.; Breen, B.; Barnes, P. R. F.; Durrant, J. R.; Law, C.; et al. The Mechanism Behind the Beneficial Effect of Light Soaking on Injection Efficiency and Photocurrent in Dye Sensitized Solar Cells. *Energy Environ. Sci.* **2011**, *4*, 3494−3501.
(37) Listorti, A.; O'Regan, B.; Durrant, J. R. Electron Transfer Dynamics in Dye-Sensitized Solar Cells. *Chem. Mater.* **2011**, *23*, 3381−3399.
(38) Anderson, N. A.; Lian, T. Ultrafast Electron Transfer at the Molecule-Semiconductor Nanoparticle Interface. *Annu. Rev. Phys. Chem.* **2004**, *56*, 491−519.
(39) Lobello, M. G.; Fantacci, S.; De Angelis, F. Computational Spectroscopy Characterization of the Species Involved in Dye Oxidation and Regeneration Processes in Dye-Sensitized Solar Cells. *J. Phys. Chem. C* **2011**, *115*, 18863−18872.

(40) Koops, S. E.; Barnes, P. R. F.; O'Regan, B. C.; Durrant, J. R. Kinetic Competition in a Coumarin Dye-Sensitized Solar Cell: Injection and Recombination Limitations Upon Device Performance. *J. Phys. Chem. C* **2010**, *114*, 8054−8061.
(41) Pastore, M.; De Angelis, F. Computational Modelling of TiO_2 Surfaces Sensitized by Organic Dyes With Different Anchoring Groups: Adsorption Modes, Electronic Structure and Implication for Electron Injection/Recombination. *Phy. Chem. Chem. Phys.* **2012**, *14*, 920−928.
(42) Koops, S. E.; O'Regan, B. C.; Barnes, P. R. F.; Durrant, J. R. Parameters Influencing the Efficiency of Electron Injection in Dye-Sensitized Solar Cells. *J. Am. Chem. Soc.* **2009**, *131*, 4808−4818.
(43) Cheng, J.; Sprik, M. Aligning Electronic Energy Levels at the TiO_2/H_2O Interface. *Phys. Rev. B* **2010**, *82*, 081406.
(44) Rothenberger, G.; Fitzmaurice, D.; Grätzel, M. Spectroscopy of Conduction Band Electrons in Transparent Metal Oxide Semiconductor Films: Optical Determination of the Flatband Potential of Colloidal Titanium Dioxide Films. *J. Phys. Chem.* **1992**, *96*, 5983−5986.
(45) Boschloo, G.; Fitzmaurice, D. Electron Accumulation in Nanostructured TiO_2 (Anatase) Electrodes. *J. Phys. Chem. B* **1999**, *103*, 7860−7868.
(46) Redmond, G.; Fitzmaurice, D. Spectroscopic Determination of Flatband Potentials for Polycrystalline Titania Electrodes in Non-aqueous Solvents. *J. Phys. Chem.* **1993**, *97*, 1426−1430.
(47) Liu, Y.; Hagfeldt, A.; Xiao, X.-R.; Lindquist, S.-E. Investigation of Influence of Redox Species on the Interfacial Energetics of a Dye-Sensitized Nanoporous TiO_2 Solar Cell. *Sol. Energy Mater. Sol. Cells* **1998**, *55*, 267−281.
(48) Watson, D. F.; Meyer, G. J. Cation Effects in Nanocrystalline Solar Cells. *Coord. Chem. Rev.* **2004**, *248*, 1391−1406.
(49) Furube, A.; Katoh, R.; Hara, K.; Sato, T.; Murata, S.; Arakawa, H.; Tachiya, M. Lithium Ion Effect on Electron Injection from a Photoexcited Coumarin Derivative Into a TiO_2 Nanocrystalline Film Investigated by Visible-to-IR Ultrafast Spectroscopy. *J. Phys. Chem. B* **2005**, *109*, 16406−16414.
(50) Zhang, J.; F. Hughes, T.; Steigerwald, M.; Brus, L.; A. Friesner, R. Realistic Cluster Modeling of Electron Transport and Trapping in Solvated TiO_2 Nanoparticles. *J. Am. Chem. Soc.* **2012**, *134*, 12028−12042.
(51) Olson, C. L.; Nelson, J.; Islam, M. S. Defect Chemistry, Surface Structures, and Lithium Insertion in Anatase TiO_2. *J. Phys Chem. B* **2006**, *110*, 9995−10001.
(52) Enright, B.; Redmond, G.; Fitzmaurice, D. Spectroscopic Determination of Flatband Potentials for Polycrystalline TiO_2 Electrodes in Mixed Solvent Systems. *J. Phys. Chem.* **1994**, *98*, 6195−6200.
(53) Zaban, A.; Ferrere, S.; Sprague, J.; Gregg, B. A. pH-Dependent Redox Potential Induced in a Sensitizing Dye by Adsorption Onto TiO_2. *J. Phys. Chem. B* **1997**, *101*, 55−57.
(54) Zaban, A.; Ferrere, S.; Gregg, B. A. Relative Energetics at the Semiconductor/Sensitizing Dye/Electrolyte Interface. *J. Phys. Chem. B* **1998**, *102*, 452−460.
(55) Kalyanasundaram, K.; Vlachopoulos, N.; Krishnan, V.; Monnier, A.; Grätzel, M. Sensitization of Titanium Dioxide in the Visible Light Region Using Zinc Porphyrins. *J. Phys. Chem.* **1987**, *91*, 2342−2347.
(56) Yan, S. G.; Hupp, J. T. Semiconductor-Based Interfacial Electron-Transfer Reactivity: Decoupling Kinetics from pH-Dependent Band Energetics in a Dye-Sensitized Titanium Dioxide/Aqueous Solution System. *J. Phys. Chem.* **1996**, *100*, 6867−6870.
(57) Qu, P.; Meyer, G. J. Proton-Controlled Electron Injection from Molecular Excited States to the Empty States in Nanocrystalline TiO_2. *Langmuir* **2001**, *17*, 6720−6728.
(58) Wang, Z.-S.; Zhou, G. Effect of Surface Protonation of TiO_2 on Charge Recombination and Conduction Band Edge Movement in Dye-Sensitized Solar Cells. *J. Phys. Chem. C* **2009**, *113*, 15417−15421.
(59) Wang, Z.-S.; Yamaguchi, T.; Sugihara, H.; Arakawa, H. Significant Efficiency Improvement of the Black Dye-Sensitized Solar Cell through Protonation of TiO_2 Films. *Langmuir* **2005**, *21*, 4272−4276.
(60) Jung, H. S.; Lee, J.-K.; Lee, S.; Hong, K. S.; Shin, H. Acid Adsorption on TiO_2 Nanoparticles−An Electrochemical Properties Study. *J. Phys. Chem. C* **2008**, *112*, 8476−8480.
(61) Labat, F.; Le Bahers, T.; Ciofini, I.; Adamo, C. First-Principles Modeling of Dye-Sensitized Solar Cells: Challenges and Perspectives. *Acc. Chem. Res.* **2012**, *45*, 1268−1277.
(62) Agrawal, S.; Leijtens, T.; Ronca, E.; Pastore, M.; Snaith, H.; De Angelis, F. Modeling the Effect of Ionic Additives on the Optical and Electronic Properties of a Dye-Sensitized TiO_2 Heterointerface: Absorption, Charge Injection and Aggregation. *J. Mater. Chem. A* **2013**, *1*, 14675−14685.
(63) Abrusci, A.; Kumar, R.; Al-Hashimi, M.; Heeney, M.; Petrozza, A.; Snaith, H. Influence of Ion Induced Local Coulomb Field and Polarity on Charge Generation and Efficiency in Poly(3-Hexylthiophene)-Based Solid-State Dye-Sensitized Solar Cells. *Adv. Func. Mater.* **2011**, *21*, 2571−2579.
(64) Zhu, R.; Jiang, C.-Y.; Liu, B.; Ramakrishna, S. Highly Efficient Nanoporous TiO_2-Polythiophene Hybrid Solar Cells Based on Interfacial Modification Using a Metal-Free Organic Dye. *Adv. Mater.* **2009**, *21*, 994−1000.
(65) Yang, X.; Zhang, S.; Zhang, K.; Liu, J.; Qin, C.; Chen, H.; Islam, A.; Han, L. Coordinated Shifts of Interfacial Energy Levels: Insight Into Electron Injection in Highly Efficient Dye-Sensitized Solar Cells. *Energy Environ. Sci.* **2013**, *6*, 3637−3645.
(66) Marotta, G.; Lobello, M. G.; Anselmi, C.; Barozzino Consiglio, G.; Calamante, M.; Mordini, A.; Pastore, M.; De Angelis, F. An Integrated Experimental and Theoretical Approach to the Spectroscopy of Organic-Dye-Sensitized TiO_2 Heterointerfaces: Disentangling the Effects of Aggregation, Solvation, and Surface Protonation. *ChemPhysChem* **2014**, DOI: 10.1002/cphc.201300923.
(67) Marotta, G.; Lobello, M. G.; Anselmi, C.; Barozzino Consiglio, G.; Calamante, M.; Mordini, A.; Pastore, M.; De Angelis, F. An Integrated Experimental and Theoretical Approach to the Spectroscopy of Organic Dye-Sensitized TiO_2 Heterointerfaces: Disentangling the Effects of Aggregation, Solvation and Surface Protonation. *ChemPhysChem* **2013**.
(68) Muscat, J. P.; Newns, D. M. Chemisorption on Metals. *Prog. Surf. Sci.* **1978**, *9*, 1−43.
(69) Kondov, I.; Čížek, M.; Benesch, C.; Wang, H.; Thoss, M. Quantum Dynamics of Photoinduced Electron-Transfer Reactions in Dye−Semiconductor Systems: First-Principles Description and Application to Coumarin 343−TiO_2. *J. Phys. Chem. C* **2007**, *111*, 11970−11981.
(70) Li, J.; Wang, H.; Persson, P.; Thoss, M. Photoinduced Electron Transfer Processes in Dye-Semiconductor Systems with Different Spacer Groups. *J. Chem. Phys.* **2012**, *137*, 22A529-1−22A529-16.
(71) Kim, S.; Lee, J. K.; Kang, S. O.; Ko, J.; Yum, J. H.; Fantacci, S.; De Angelis, F.; Di Censo, D.; Nazeeruddin, M. K.; Grätzel, M. Molecular Engineering of Organic Sensitizers for Solar Cell Applications. *J. Am. Chem. Soc.* **2006**, *128*, 16701−16707.
(72) Chen, P.; Yum, J. H.; De Angelis, F.; Mosconi, E.; Fantacci, S.; Moon, S.-J.; Baker, R. H.; Ko, J.; Nazeeruddin, M. K.; Grätzel, M. High Open-Circuit Voltage Solid-State Dye-Sensitized Solar Cells with Organic Dye. *Nano Lett.* **2009**, *9*, 2487−2492.
(73) Pastore, M.; Fantacci, S.; De Angelis, F. Modeling Excited States and Alignment of Energy Levels in Dye-Sensitized Solar Cells: Successes, Failures, and Challenges. *J. Phys Chem. C* **2013**, *117*, 3685−3700.
(74) Pastore, M.; De Angelis, F. Computational Modelling of TiO_2 Surfaces Sensitized by Organic Dyes with Different Anchoring Groups: Adsorption Modes, Electronic Structure and Implication for Electron Injection/Recombination. *Phys. Chem. Chem. Phys.* **2012**, *14*, 920−928.
(75) De Angelis, F.; Fantacci, S.; Selloni, A.; Nazeeruddin, M. K.; Grätzel, M. First-Principles Modeling of the Adsorption Geometry and Electronic Structure of Ru(II) Dyes on Extended TiO_2 Substrates for Dye-Sensitized Solar Cell Applications. *J. Phys. Chem. C* **2010**, *114*, 6054−6061.
(76) Vittadini, A.; Selloni, A.; Rotzinger, F. P.; Grätzel, M. Structure and Energetics of Water Adsorbed at TiO_2 Anatase (101) and (001) Surfaces. *Phys. Rev. Lett.* **1998**, *81*, 2954−2957.
(77) Ito, S.; Nazeeruddin, M. K.; Liska, P.; Comte, P.; Charvet, R.; Péchy, P.; Jirousek, M.; Kay, A.; Zakeeruddin, S. M.; Grätzel, M. Photovoltaic Characterization of Dye-Sensitized Solar Cells: Effect of

Device Masking on Conversion Efficiency. *Prog. Photovoltaics* **2006**, *14*, 589−601.
(78) Weng, Y.-X.; Wang, Y.-Q.; Asbury, J. B.; Ghosh, H. N.; Lian, T. Back Electron Transfer from TiO_2 Nanoparticles to $Fe^{III}(CN)_6^{3-}$: Origin of Non-Single-Exponential and Particle Size Independent Dynamics. *J. Phys. Chem. B* **2000**, *104*, 93−104.
(79) Khoudiakov, M.; Parise, A. R.; Brunschwig, B. S. Interfacial Electron Transfer in $Fe^{II}(CN)_6^{4-}$−Sensitized TiO_2 Nanoparticles: A Study of Direct Charge Injection by Electroabsorption Spectroscopy. *J. Am. Chem. Soc.* **2003**, *125*, 4637−4642.
(80) De Angelis, F.; Fantacci, S.; Mosconi, E.; Nazeeruddin, M. K.; Grätzel, M. Absorption Spectra and Excited State Energy Levels of the N719 Dye on TiO_2 in Dye-Sensitized Solar Cell Models. *J. Phys. Chem. C* **2011**, *115*, 8825−8831.
(81) te Velde, G.; Bickelhaupt, F. M.; Baerends, E. J.; Fonseca Guerra, C.; van Gisbergen, S. J. A.; Snijders, J. G.; Ziegler, T. Chemistry with ADF. *J. Comput. Chem.* **2001**, *22*, 931−967.
(82) Perdew, J. P.; Burke, K.; Ernzerhof, M. Generalized Gradient Approximation Made Simple. *Phys. Rev. Lett.* **1996**, *77*, 3865−3868.
(83) Cohen-Tannoudji, C.; Diu, B.; Laloe, F. *Quantum Mechanics*; J. Wiley & Sons: Paris, 1977; Vol. 2.
(84) Persson, P.; Lundqvist, M. J.; Ernstorfer, R.; Goddard, W. A.; Willig, F. Quantum Chemical Calculations of the Influence of Anchor-Cum-Spacer Groups on Femtosecond Electron Transfer Times in Dye-Sensitized Semiconductor Nanocrystals. *J. Chem. Theory Comput.* **2006**, *2*, 441−451.
(85) Lundqvist, M. J.; Nilsing, M.; Lunell, S.; Åkermark, B.; Persson, P. Spacer and Anchor Effects on the Electronic Coupling in Ruthenium-bis-Terpyridine Dye-Sensitized TiO_2 Nanocrystals Studied by DFT. *J. Phys Chem. B* **2006**, *110*, 20513−20525.
(86) Persson, P.; Lundqvist, M. J. Calculated Structural and Electronic Interactions of the Ruthenium Dye N3 with a Titanium Dioxide Nanocrystal. *J. Phys. Chem. B* **2005**, *109*, 11918−11924.
(87) Persson, P.; Lunell, S.; Ojamäe, L. Quantum Chemical Prediction of the Adsorption Conformations and Dynamics at HCOOH-Covered ZnO(1010) Surfaces. *Int. J. Quantum Chem.* **2002**, *89*, 172−180.
(88) Schäfer, A.; Horn, H.; Ahlrichs, R. Fully Optimized Contracted Gaussian Basis Sets for Atoms Li to Kr. *J. Chem. Phys.* **1992**, *97*, 2571−2577.
(89) Schäfer, A.; Huber, C.; Ahlrichs, R. Fully Optimized Contracted Gaussian Basis Sets of Triple Zeta Valence Quality for Atoms Li to Kr. *J. Chem. Phys.* **1994**, *100*, 5829−5835.
(90) Barone, V.; Cossi, M. Quantum Calculation of Molecular Energies and Energy Gradients in Solution by a Conductor Solvent Model. *J. Phys. Chem. A* **1998**, *102*, 1995−2001.
(91) Cossi, M.; Rega, N.; Scalmani, G.; Barone, V. Energies, Structures, and Electronic Properties of Molecules in Solution with the C-PCM Solvation Model. *J. Comput. Chem.* **2003**, *24*, 669−681.
(92) Frisch, M. J.; Trucks, G. W.; Schlegel, H. B.; Scuseria, G. E.; Robb, M. A.; Cheeseman, J. R.; Scalmani, G.; Barone, V.; Mennucci, B.; Petersson, G. A.; et al. *Gaussian 09*, revision A.02; Gaussian, Inc.: Wallingford, CT, 2009.
(93) Hao, S.; Wu, J.; Fan, L.; Huang, Y.; Lin, J.; Wei, Y. The Influence of Acid Treatment of TiO_2 Porous Film Electrode on Photoelectric Performance of Dye-Sensitized Solar Cell. *Sol. Energy* **2004**, *76*, 745−750.
(94) Lundqvist, M. J.; Nilsing, M.; Persson, P.; Lunel, S. DFT Study of Bare and Dye-Sensitized TiO_2 Clusters and Nanocrystals. *Int. J. Quantum Chem.* **2006**, *106*, 3214−3234.
(95) Jones, D. R.; Troisi, A. A Method to Rapidly Predict the Charge Injection Rate in Dye Sensitized Solar Cells. *Phys. Chem. Chem. Phys.* **2010**, *12*, 4625−4634.
(96) Martsinovich, N.; Troisi, A. High-Throughput Computational Screening of Chromophores for Dye-Sensitized Solar Cells. *J. Phys. Chem. C* **2011**, *115*, 11781−11792.
(97) Wiberg, J.; Marinado, T.; Hagberg, D. P.; Sun, L.; Hagfeldt, A.; Albinsson, B. Distance and Driving Force Dependencies of Electron Injection and Recombination Dynamics in Organic Dye-Sensitized Solar Cell. *J. Phys. Chem. B* **2010**, *114*, 14358−14363.
(98) Hara, K.; Sato, T.; Katoh, R.; Furube, A.; Ohga, Y.; Shinpo, A.; Suga, S.; Sayama, K.; Sugihara, H.; Arakawa, H. Molecular Design of Coumarin Dyes for Efficient Dye-Sensitized Solar Cells. *J. Phys. Chem. B* **2003**, *107*, 597−606.
(99) Asbury, J. B.; Hao, E.; Wang, Y.; Ghosh, H. N.; Lian, T. Ultrafast Electron Transfer Dynamics from Molecular Adsorbates to Semiconductor Nanocrystalline Thin Films. *J. Phys. Chem. B* **2001**, *105*, 4545−4557.
(100) Cioslowski, J. A New Population Analysis Based on Atomic Polar Tensors. *J. Am. Chem. Soc.* **1989**, *111*, 8333−8336.
(101) Hagberg, D. P.; Edvinsson, T.; Marinado, T.; Boschloo, G.; Hagfeldt, A.; Sun, L. A Novel Organic Chromophore for Dye-Sensitized Nanostructured Solar Cells. *Chem. Commun.* **2006**, No. 21, 2245−2247.
(102) Wang, Z.-S.; Li, F.-Y.; Huang, C.-H. Photocurrent Enhancement of Hemicyanine Dyes Containing RSO_3^- Group through Treating TiO_2 Films with Hydrochloric Acid. *J. Phys. Chem. B* **2001**, *105*, 9210−9217.